Deriving pedotransfer functions for soil quartz fraction in southern France from reverse modelling

Jean-Christophe Calvet, Noureddine Fritz,
Christine Berne, Bruno Piguet, William Maurel, and Catherine Meurey

CNRM, UMR 3589 (Météo-France, CNRS), Toulouse, France

27 October 2016

Abstract

The quartz fraction in soils is a key parameter of soil thermal conductivity models. Because it is difficult to measure the quartz fraction in soils, this information is usually unavailable. This source of uncertainty impacts the simulation of sensible heat flux, evapotranspiration, and land surface temperature in numerical simulations of the Earth system. Improving the estimation of soil quartz fraction is needed for practical applications in meteorology, hydrology, and climate modelling. This paper investigates the use of long time series of routine ground observations made in weather stations to retrieve the soil quartz fraction. Profile soil temperature and water content were monitored at 21 weather stations in southern France. Soil thermal diffusivity was derived from the temperature profiles. Using observations of bulk density, soil texture, and fractions of gravel and soil organic matter, soil heat capacity and thermal conductivity were estimated. The quartz fraction was inversely estimated using an empirical geometric mean thermal conductivity model. Several pedotransfer functions for estimating quartz content from gravimetric or volumetric fractions of soil particles (e.g. sand) were analysed. The soil volumetric fraction of quartz (f_q) was systematically better correlated to soil characteristics than the gravimetric fraction

of quartz. More than 60 % of the variance of f_q could be explained using indicators based on the sand fraction. It was shown that soil organic matter and (or) gravels may have a marked impact on thermal conductivity values depending on which predictor of f_q is used. For the grassland soils examined in this study, the ratio of sand to soil organic matter fractions was the best predictor of f_q, followed by the gravimetric fraction of sand. An error propagation analysis and a comparison with independent data from other tested models showed that the gravimetric fraction of sand is the best predictor of f_q when a larger variety of soil types is considered.

1. Introduction

Soil moisture is the main driver of temporal changes in values of the soil thermal conductivity (Sourbeer and Loheide, 2015). The latter is a key variable in land surface models (LSMs) used in hydrometeorology or in climate models, for the simulation of the vertical profile of soil temperature in relation to soil moisture (Subin et al., 2013). Shortcomings in soil thermal conductivity models tend to limit the impact of improving the simulation of soil moisture and snowpack in LSMs (Lawrence and Slater, 2008; Decharme et al. 2016). Models of the thermal conductivity of soils are affected by uncertainties, especially in the representation of the impact of soil properties such as the volumetric fraction of quartz (f_q), soil organic matter, and gravels (Farouki, 1986; Chen et al., 2012). As soil organic matter (SOM) and gravels are often neglected in LSMs, the soil thermal conductivity models used in most LSMs represent the mineral fine earth, only. Nowadays, f_q estimates are not given in global digital soil maps and it is often assumed that this quantity is equal to the fraction of sand (Peters-Lidard et al., 1998).

Soil thermal properties are characterized by two key variables: the soil volumetric heat capacity (C_h), and the soil thermal conductivity (λ), in $Jm^{-3}K^{-1}$ and $Wm^{-1}K^{-1}$, respectively. Provided the volumetric fractions of moisture, minerals and organic matter are known, C_h can be calculated easily. The estimation of λ relies on empirical models and is affected by uncertainties (Peters-Lidard et al., 1998; Tarnawski et al., 2012). The construction and the verification of the λ models is not easy. The λ values of undisturbed soils are difficult to directly observe. They are often measured in the lab on perturbed soil samples (Abu-Hamdeh et al., 2000; Lu et al., 2007). Although recent advances in line-source probe and heat pulse methods have made it easier to monitor soil thermal conductivity in the field (Bristow et al., 1994; Zhang et al., 2014), such measurements are currently not made in operational meteorological networks. Moreover, for given soil moisture conditions, λ depends to a large extent on the fraction of soil minerals presenting high thermal conductivities such as quartz, hematite, dolomite or pyrite (Côté and Conrad, 2005). In mid-latitude regions of the world, quartz is the main driver of λ. The information on quartz fraction in a soil is usually unavailable as it can only be measured using X-ray diffraction (XRD) or X-ray fluorescence (XRF) techniques. These techniques are difficult to implement because the sensitivity to quartz is low. In practise, using XRD and XRF together is needed to improve the accuracy of the measurements (Schönenberger et al., 2012). This lack of observations has a major effect on the accuracy of thermal conductivity models and their applications (Bristow, 1998).

Most of the Land Surface Models (LSMs) currently used in meteorology and hydrometeorology simulate λ following the approach proposed by Peters-Lidard et al. (1998). This approach consists of an updated version of the Johansen (1975) model, and assumes that the gravimetric fraction of quartz (Q) is equal to the gravimetric fraction of sand within mineral fine earth. This is a strong assumption, as some sandy soils (e.g. calcareous sands) may contain little quartz, and as quartz may be found in the silt and clay fractions of the soil minerals (Schönenberger et al., 2012). Moreover, the λ models used in most LSMs represent only the mineral fine earth. Yang et al. (2005) and Chen et al. (2012) have shown the importance of accounting for SOM and gravels in λ models for organic top soil layers of grasslands of the Tibetan plateau.

The main goals of this study are to (1) assess the feasibility of using routine automatic soil temperature profile sub-hourly measurements (one observation every 12 minutes) to retrieve instantaneous soil thermal diffusivity values at a depth of 0.10 m; (2) retrieve instantaneous λ values from the soil thermal diffusivity estimates, accounting for the impact of soil vertical heterogeneities; (3) obtain, from reverse modelling, the quartz fraction together with soil thermal conductivity at saturation (λ_{sat}); (4) assess the impact of gravels and SOM on λ_{sat}; (5) derive pedotransfer functions for the soil quartz fraction.

For this purpose, we use the data from 21 weather stations of the Soil Moisture Observing System – Meteorological Automatic Network Integrated Application (SMOSMANIA) network (Calvet et al., 2007) in southern France. The soil temperature and the soil moisture probes are buried in the enclosure around each weather station. Most of these stations are located in agricultural areas. However, the vegetation cover in the enclosure around the stations consists of grass. Along the Atlantic-Mediterranean transect formed by the SMOSMANIA network (Fig. 1), the grass land cover fraction ranges between 10 % and 40 % (Zakharova et al., 2012). Various mineral soil types can be found along this transect, ranging from sand to clay and silt loam (see Supplement 1). During the installation of the probes, we collected soil samples which were used to determine soil characteristics: soil texture, soil gravel content, soil organic matter, and bulk density.

Using this information together with soil moisture, λ values are derived from soil thermal diffusivity and heat capacity. The response of λ to soil moisture is investigated. The feasibility of modelling the λ value at saturation (λ_{sat}) with or without using SOM and gravel fraction observations is assessed using a geometric mean empirical thermal conductivity model based on Lu et al. (2007). The volumetric fraction of quartz, f_q, is retrieved by reverse modelling together with Q. Pedotransfer functions are further proposed for estimating quartz content from soil texture information.

The field data and the method to retrieve λ values are presented in Sect. 2. The λ and f_q retrievals are presented in Sect. 3 together with a sensitivity analysis of λ_{sat} to SOM and gravel fractions. Finally, the results are discussed in Sect. 4, and the main conclusions are summarized in Sect. 5. Technical details are given in Supplements.

2. Data and methods

2.1. The SMOSMANIA data

The SMOSMANIA network was developed by Calvet et al. (2007) in southern France. The main purposes of SMOSMANIA are to (1) validate satellite-derived soil moisture products (Parrens et al., 2012); (2) assess land surface models used in hydrological models (Draper et al., 2011) and in meteorological models (Albergel et al., 2010); and (3) monitor the impact of climate change on water resources and droughts (Laanaia et al., 2016). The station network forms a transect between the Atlantic coast and the Mediterranean sea (Fig. 1). It consists of pre-existing automatic weather stations operated by Meteo-France, upgraded with four soil moisture probes at four depths: 0.05 m, 0.10 m, 0.20 m, and 0.30 m. Twelve SMOSMANIA stations were activated in 2006 in southwestern France. In 2008, nine more stations were installed along the Mediterranean coast, and the whole network (21 stations) was gradually equipped with temperature sensors at the same depths as soil moisture probes. The soil moisture and soil temperature probes consisted of Thetaprobe ML2X and PT100 sensors, respectively. Soil moisture and soil temperature observations were made every 12 minutes at four depths. The soil temperature observations were recorded with a resolution of 0.1 °C.

In this study, the sub-hourly measurements of soil temperature and soil moisture at a depth of 0.10 m were used, together with soil temperature measurements at 0.05 m and 0.20 m, from 1 January 2008 to 30 September 2015.

The ThetaProbe soil moisture sensors provide a voltage signal (V). In order to convert the voltage signal into volumetric soil moisture content (m^3 m^{-3}), site-specific calibration curves were developed using in situ gravimetric soil samples for all stations, and for all depths (Albergel et al., 2008). We revised the calibration in order to avoid spurious high soil moisture values during intense precipitation events. Logistics curves were used (see Supplement 1) instead of exponential curves in the previous version of the data set.

The observations from the soil moisture (48) and from the temperature (48) probes are automatically recorded every 12 minutes. The data are available to the research community through the International Soil Moisture Network web site (https://ismn.geo.tuwien.ac.at/).

Figure 2 shows soil temperature time series in wet conditions at various soil depths, for a station presenting an intermediate value of λ_{sat} (Table 2) and of soil texture (see Fig. S1.1 in Supplement

1). The impact of recording temperature with a resolution of 0.1 °C is clearly visible at all depths as this causes a levelling of the curves.

2.2. Soil characteristics

In general, the stations are located on formerly cultivated fields and the soil in the enclosure around the stations is covered with grass. Soil properties were measured at each station by an independent laboratory we contracted (INRA-Arras) from soil samples we collected during the installation of the probes. The 21 stations cover a very large range of soil texture characteristics. For example, SBR is located on a sandy soil, PRD on a clay loam, and MNT on a silt loam (Table 1 and Supplement 1). Other properties such as the gravimetric fraction of SOM and of gravels were determined from the soil samples. Table 1 shows that 12 soils present a volumetric gravel content (f_{gravel}) larger than 15 %. Among these, 3 soils (at PRD, BRN, and MJN) have f_{gravel} values larger than 30 %.

In addition, we measured bulk density (ρ_{d}) using undisturbed oven-dried soil samples we collected using metal cylinders of known volume (about 7×10^{-4} m^3, see Fig. S1.10 in the Supplement).

The porosity values at a depth of 0.10 m are listed in Table 1 together with gravimetric and volumetric fractions of soil particle-size ranges (sand, clay, silt, gravel) and SOM. The porosity, or soil volumetric moisture at saturation (θ_{sat}), is derived from the bulk dry density ρ_{d}, with soil texture and soil organic matter observations as:

$$\theta_{sat} = 1 - \rho_d \left[\frac{m_{sand} + m_{clay} + m_{silt} + m_{gravel}}{\rho_{\min}} + \frac{m_{SOM}}{\rho_{SOM}} \right]$$

or

$$\theta_{sat} = 1 - f_{sand} - f_{clay} - f_{silt} - f_{gravel} - f_{SOM} \quad (1)$$

where m_x (f_x) represents the gravimetric (volumetric) fraction of the soil component *x*. The f_x values are derived from the measured gravimetric fractions, multiplied by the ratio of ρ_d observations to ρ_x, the density of each soil component *x*. Values of ρ_{SOM} = 1300 kg m^{-3} and ρ_{min} = 2660 kg m^{-3} are used for soil organic matter, and soil minerals, respectively.

2.3. Retrieval of soil thermal diffusivity

The soil thermal diffusivity (D_h) is expressed in m^{2}s^{-1} and is defined as:

$$D_h = \frac{\lambda}{C_h} \quad (2)$$

We used a numerical method to retrieve instantaneous values of D_h at a depth of 0.10 m using three soil temperature observations at 0.05 m, 0.10 m and 0.20 m, performed every 12 minutes, by solving the Fourier thermal diffusion equation. The latter can be written as:

$$C_h \frac{\partial T}{\partial t} = \frac{\partial}{\partial z}\left(\lambda \frac{\partial T}{\partial z}\right) \quad (3).$$

Given that soil properties are relatively homogeneous on the vertical (Sect. 2.1), values of D_h can be derived from the Fourier one-dimensional law:

$$\frac{\partial T}{\partial t} = D_h \frac{\partial^2 T}{\partial z^2} \quad (4).$$

However, large differences in soil bulk density, from the top soil layer to deeper soil layers were observed for some soils (see Supplement 1). In order to limit this effect as much as possible, we only used the soil temperature data presenting a relatively low vertical gradient close to the soil surface, where most differences with deeper layers are found. This data sorting procedure is described in Supplement 2.

Given that three soil temperatures T_i (i ranging from 1 to 3) are measured at depths z_1 = –0.05 m, z_2 = –0.10 m, and z_3 = –0.20 m, the soil diffusivity D_{hi} at $z_i = z_2$ = –0.10 m can be obtained by solving the one-dimensional heat equation, using a finite difference method based on the implicit Crank-Nicolson scheme (Crank and Nicolson, 1996). When three soil depths are considered, z_{i-1}, z_i, z_{i+1}, the change in soil temperature T_i at depth z_i, from time t_{n-1} to time t_n, within the time interval $\Delta t = t_n - t_{n-1}$ can be written as:

$$\frac{T_i^n - T_i^{n-1}}{\Delta t} = D_{hi}\left[\frac{1}{2}\left(\frac{\gamma_{i+1}^n - \gamma_i^n}{\Delta z_m}\right) + \frac{1}{2}\left(\frac{\gamma_{i+1}^{n-1} - \gamma_i^{n-1}}{\Delta z_m}\right)\right] \quad \text{with}$$

$$\gamma_i^n = \frac{T_i^n - T_{i-1}^n}{\Delta z_i}, \; \Delta z_m = \frac{\Delta z_i + \Delta z_{i+1}}{2}, \text{ and } \Delta z_i = z_i - z_{i-1} \qquad (5).$$

In this study, Δz_i = –0.05 m, Δz_{i+1} = –0.10 m, and a value of Δt = 2880 s (48 minutes) is used.

It is important to ensure that D_h retrievals are related to diffusion processes only and not to the transport of heat by water infiltration or evaporation (Parlange et al., 1998 ; Schelde et al., 1998). Therefore, only situations for which changes in soil moisture at all depths do not exceed 0.001 m^3m^{-3} within the Δt time interval are considered.

2.4. From soil diffusivity to soil thermal conductivity

The observed soil properties and volumetric soil moisture are used to calculate the soil volumetric heat capacity C_h at a depth of 0.10 m, using the de Vries (1963) mixing model. The C_h values, in units of $Jm^{-3}K^{-1}$, are calculated as:

$$C_h = \theta C_{h\,water} + f_{\min} C_{h\min} + f_{SOM}\, C_{hSOM} \tag{6}$$

where θ and $f_{\min}$ represent the volumetric soil moisture and the volumetric fraction of soil minerals, respectively. Values of 4.2×10^6 $Jm^{-3}K^{-1}$, 2.0×10^6 $Jm^{-3}K^{-1}$, and 2.5×10^6 $Jm^{-3}K^{-1}$, are used for $C_{h\mathrm{water}}$, $C_{h\mathrm{min}}$, $C_{h\mathrm{SOM}}$, respectively.

The λ values at 0.10 m are then derived from the D_h and C_h estimates (Eq. (2)).

2.5. Soil thermal conductivity model

Various approaches can be used to simulate thermal conductivity of unsaturated soils (Dong et al., 2015). We used an empirical approach based on thermal conductivity values in dry conditions and at saturation.

In dry conditions, soils present low thermal conductivity values (λ_dry). Experimental evidence shows that λ_dry is negatively correlated with porosity. For example, Lu et al. (2007) give:

$$\lambda_{dry} = 0.51 - 0.56\times\theta_{sat} \qquad \text{(in } Wm^{-1}K^{-1}\text{)} \tag{7}$$

When soil pores are gradually filled with water, λ tends to increase towards a maximum value at saturation (λ_sat). Between dry and saturation conditions, λ is expressed as:

$$\lambda = \lambda_{dry} + K_e\left(\lambda_{sat} - \lambda_{dry}\right) \tag{8}$$

where, K_e is the Kersten number (Kersten, 1949). The latter is related to the volumetric soil moisture, θ, i.e. to the degree of saturation (S_d). We used the formula recommended by Lu et al. (2007):

$$K_e = \exp\left\{\alpha\left(1 - S_d^{(\alpha - 1.33)}\right)\right\},$$

with $\alpha = 0.96$ for $Mn_{sand} \geq 0.4$ kg kg^{-1}, $\alpha = 0.27$ for $Mn_{sand} < 0.4$ kg kg^{-1}, and

$$S_d = \theta / \theta_{sat} \tag{9}$$

Mn_{sand} represents the sand mass fraction of mineral fine earth (values are given in Supplement 1). The geometric mean equation for λ_{sat} proposed by Johansen (1975) for the mineral components of the soil can be generalized to include the SOM thermal conductivity (Chen et al., 2012) as:

$$\ln(\lambda_{sat}) = f_q \ln(\lambda_q) + f_{other} \ln(\lambda_{other}) + \theta_{sat} \ln(\lambda_{water}) + f_{SOM} \ln(\lambda_{SOM}) \tag{10}$$

where f_q is the volumetric fraction of quartz, and $\lambda_q = 7.7$ Wm^{-1}K^{-1}, $\lambda_{water} = 0.594$ Wm^{-1}K^{-1}, $\lambda_{SOM} = 0.25$ Wm^{-1}K^{-1} are the thermal conductivities of quartz, water and SOM, respectively. The λ_{other} term corresponds to the thermal conductivity of soil minerals other than quartz. Following Peters-Lidard et al. (1998), λ_{other} is taken as 2.0 Wm^{-1}K^{-1} for soils with $Mn_{sand} > 0.2$ kg kg^{-1}, and 3.0 Wm^{-1}K^{-1} otherwise. In this study $Mn_{sand} > 0.2$ kg kg^{-1} for all soils, except for URG, PRG, and CDM. The volumetric fraction of soil minerals other than quartz is defined as:

$$f_{other} = 1 - f_q - \theta_{sat} - f_{SOM}$$

with $f_q = Q \times (1 - \theta_{sat})$ (11)

2.6. Reverse modelling

The λ_{sat} values are retrieved through reverse modelling using the λ model described above (Eqs. (7)-(11)). This model is used to produce simulations of λ at the same soil moisture conditions as those encountered for the λ values derived from observations in Sect. 2.4. For a given station, a set of 401 simulations is produced for λ_{sat} ranging from 0 $Wm^{-1}K^{-1}$ to 4 $Wm^{-1}K^{-1}$, with a resolution of 0.01 $Wm^{-1}K^{-1}$. The λ_{sat} retrieval corresponds to the λ simulation presenting the lowest root mean square difference (RMSD) value with respect to the λ observations. Only λ observations for S_d values higher than 0.4 are used because in dry conditions: (1) conduction is not the only mechanism for heat exchange in soils, as the convective water vapour flux may become significant (Schelde et al., 1998; Parlange et al. 1998); (2) the K_e functions found in the literature display more variability; and, (3) the λ_{sat} retrievals are more sensitive to uncertainties in λ observations. The threshold value of S_d = 0.4 results from a compromise between the need of limiting the influence of convection, of the shape of the K_e function on the retrieved values of λ_{sat}, and of using as many observations as possible in the retrieval process. Moreover, the data filtering technique to limit the impact of soil heterogeneities, described in Supplement 2, is used to select valid λ observations.

Finally, the f_q value is derived from the retrieved λ_{sat} solving Eq. (10).

2.7. Scores

Pedotransfer functions for quartz and λ_{sat} are evaluated using the following scores:

- the Pearson correlation coefficient (r), and the squared correlation coefficient (r^2) is used to assess the fraction of explained variance,

- the RMSD,
- the Mean Absolute Error (MAE), i.e. the mean of absolute differences,
- the mean bias, i.e. the mean of differences.

In order to test the predictive and generalization power of the pedotransfer regression equations, a simple bootstrapping resampling technique is used. It consists in calculating a new estimate of f_q for each soil using the pedotransfer function obtained without using this specific soil. Gathering these new f_q estimates, one can calculate new scores with respect to the retrieved f_q values. Also, this method provides a range of possible values of the coefficients of the pedotransfer function and permits assessing the influence of a given f_q retrieval on the final result.

3. Results

3.1. λ_{sat} and f_q retrievals

Retrievals of λ_{sat} and f_q could be obtained for 14 soils. Figure 3 shows retrieved and modelled λ values against the observed degree of saturation of the soil, at a depth of 0.10 m, for contrasting retrieved values of λ_{sat}, from high to low values (2.80, 1.96, 1.52, and 1.26 $Wm^{-1}K^{-1}$) at the SBR, MNT, MTM, and PRD stations, respectively.

All the obtained λ_{sat} and f_q retrievals are listed in Table 2, together with the λ RMSD values and the number of selected λ observations. For three soils (CRD, MZN, and VLV), the reverse modelling technique described in Sect. 2.6 could not be applied as not enough λ observations could be obtained for S_d values higher than 0.4. For four soils (NBN, PZN, BRZ, and MJN), all the λ retrievals were filtered out as the obtained values were influenced by heterogeneities in soil density (see Supplement 2). For the other 14 soils, λ_{sat} and f_q retrievals were obtained using a subset of 20 λ retrievals per soil, at most, corresponding to the soil temperature data presenting the lowest vertical gradient close to the soil surface (Supplement 2).

3.2 Pedotransfer functions for quartz

The f_q retrievals can be used to assess the possibility to estimate f_q using other soil characteristics, which can be easily measured. Another issue is whether volumetric or gravimetric fraction of quartz should be used. Figure 4 presents the fraction of variance (r^2) of Q and f_q explained by various indicators. A key result is that f_q is systematically better correlated to soil characteristics than Q. More than 60 % of the variance of f_q can be explained using indicators based on the sand fraction (either f_{sand} or m_{sand}). The use of other soil mineral fractions does not give good correlations, even when they are associated to the sand fraction as shown by Fig. 4. For example, the f_{gravel} and $f_{gravel}+f_{sand}$ indicators present low r^2 values of 0.04 and 0.24, respectively.

The f_q values cannot be derived directly from the indicators as illustrated by Fig. 5: assuming $f_q = f_{sand}$ tends to markedly underestimate λ_{sat}. Therefore, more elaborate pedotransfer equations are needed. They can be derived from the best indicators, using them as predictors of f_q. The modelled f_q is written as:

$$f_{qMOD} = a_0 + a_1 \times P$$

$$\text{and } f_{qMOD} \leq 1 - \theta_{sat} - f_{SOM} \tag{12}$$

where P represents the predictor of f_q.

The a_0 and a_1 coefficients are given in Table 3 for four pedotransfer functions based on the best predictors of f_q. The pedotranfer functions are illustrated in Fig. 6. The scores are displayed in Table 4. The bootstrapping indicates that the SBR sandy soil has the largest individual impact on the obtained regression coefficients. This is why the scores without SBR are also presented in Table 4.

For the m_{sand} predictor, a r^2 value of 0.56 is obtained without SBR, against a value of 0.67 when all the 14 soils are considered. An alternative to this m_{sand} pedotransfer function consists in considering only m_{sand} values smaller than 0.6 kg kg^{-1} in the regression, thus excluding the SBR soil. The corresponding predictor is called m_{sand}*. In this configuration, the sensitivity of f_q to m_{sand} is much increased (with a_1 = 0.944, against a_1 = 0.572 with SBR). For SBR, f_q is overestimated by the m_{sand}* equation but this is corrected by the f_{qMOD} limitation of Eq. (12), and in the end a better r^2 score is obtained when the 14 soils are considered (r^2 = 0.74) .

Values of r^2 larger than 0.7 are obtained for two predictors of f_q: m_{sand}/m_{SOM} and m_{sand}*. A value of r^2 = 0.65 is obtained for $1 - \theta_{sat} - f_{sand}$ (the fraction of soil solids other than sand). The m_{sand}/m_{SOM} predictor presents the best r^2 and RMSD scores in all the configurations (regression, bootstrap, and regression without SBR). Another characteristic of the m_{sand}/m_{SOM} pedotransfer function is that the confidence interval for the a_0 and a_1 coefficients derived from bootstrapping is narrower than for the other pedotransfer functions (Table 3), indicating a more robust relationship of f_q with m_{sand}/m_{SOM} than with other predictors.

An alternative way to evaluate the quartz pedotransfer functions is to compare the simulated λ_{sat} with the retrieved values presented in Table 2. Modelled values of λ_{sat} (λ_{satMOD}) can be derived from f_{qMOD} using Eq. (10) together with θ_{sat} observations. The λ_{satMOD} r^2, RMSD, and mean bias scores are given in Table 5. Again, the best scores are obtained using the m_{sand}/m_{SOM} predictor of f_q, with r^2, RMSD, and mean bias values of 0.86, 0.14 $Wm^{-1}K^{-1}$, and +0.01 $Wm^{-1}K^{-1}$, respectively (Fig. 7).

Finally, we investigated the possibility of estimating θ_{sat} from the soil characteristics listed in Table 1 and of deriving a statistical model for θ_{sat} (θ_{satMOD}). We found the following statistical relationship between θ_{satMOD}, m_{clay}, m_{silt}, and m_{SOM}:

$$\theta_{satMOD} = 0.456 - 0.0735\,\frac{m_{clay}}{m_{silt}} + 2.238\, m_{SOM} \qquad (13)$$

(r^2 = 0.48, F-test p-value = 0.0027, RMSD=0.036 m^3m^{-3}).

Volumetric fractions of soil components need to be consistent with θ_{satMOD} and can be calculated using the modelled bulk density values derived from θ_{satMOD} using Eq. (1).

Equations (10) to (13) constitute an empirical end-to-end model of λ_{sat}. Table 5 shows that using θ_{satMOD} (Eqs. (13)) instead of the θ_{sat} observations has little impact on the λ_{satMOD} scores.

3.3. Impact of gravels and SOM on λ_{sat}

Gravels and SOM are often neglected in soil thermal conductivity models used in LSMs. The Eqs. (10)-(13) empirical model obtained in Sect. 3.2 permits the assessment of the impact of f_{gravel} and f_{SOM} on λ_{sat}. Table 5 shows the impact on λ_{satMOD} scores of imposing a null value of f_{gravel} and a small value of f_{SOM} to all the soils. The combination of these assumptions is evaluated, also.

Imposing f_{SOM} = 0.013 m^{3}m^{-3} (the smallest f_{SOM} value, observed for CBR) has a limited impact on the scores, except for the m_{sand}/m_{SOM} pedotransfer function. In this case, λ_{sat} is overestimated by +0.20 Wm^{-1}K^{-1}, and r^2 drops to 0.57.

Neglecting gravels (f_{gravel} = 0 m^{3}m^{-3}) also has a limited impact but triggers the underestimation (overestimation) of λ_{sat} for the m_{sand}/m_{SOM} (m_{sand}*) pedotransfer function, by –0.12 Wm^{-1}K^{-1} (+0.11 Wm^{-1}K^{-1}).

On the other hand, it appears that combining these assumptions has a marked impact on all the pedotransfer functions. Neglecting gravels and imposing f_{SOM} = 0.013 m^{3}m^{-3} has a major impact on λ_{sat}: the modelled λ_{sat} is overestimated by all the pedotransfer functions (with a mean bias ranging from +0.16 Wm^{-1}K^{-1} to +0.24 Wm^{-1}K^{-1}) and r^2 is markedly smaller, especially for the m_{sand} and m_{sand}* pedotransfer functions. These results are illustrated in Fig. 8 in the case of the m_{sand}* pedotransfer function. Figure 8 also shows that using the θ_{sat} observations instead of θ_{satMOD} (Eq. (13)) has little impact on λ_{satMOD} (Sect. 3.2) but tends to enhance the impact of neglecting gravels. A similar result is found with the m_{sand} pedotransfer function (not shown).

4. Discussion

4.1. Can uncertainties in heat capacity estimates impact retrievals ?

In this study, the de Vries (1963) mixing model is applied to estimate soil volumetric heat capacity (Eq. (6)), and a fixed value of 2.0×10^6 Jm^{-3}K^{-1} is used for soil minerals. Soil-specific values for C_{hmin} may be more appropriate than using a constant standard value. For example, Tarara and Ham (1997) used a value of 1.92×10^6 Jm^{-3}K^{-1}. However, we did not measure this quantity and we were not able to find such values in the literature.

We investigated the sensitivity of our results to these uncertainties, considering the following minimum and maximum C_{hmin} values: $C_{hmin} = 1.92\times10^6$ J m^{-3} K^{-1} and $C_{hmin} = 2.08\times10^6$ J m^{-3} K^{-1}. The impact of changes in C_{hmin} on the retrieved values of λ_{sat} and f_q is presented in Supplement 3 (Fig. S3.1). On average, a change of + (–) 0.08×10^6 J m^{-3} K^{-1} in C_{hmin} triggers a change in λ_{sat} and f_q of + 1.7 % (– 1.8 %) and + 4.8 % (– 7.0 %), respectively.

The impact of changes in C_{hmin} on the regression coefficients of the pedotransfer functions is presented in Table 3 (last column). The impact is very small, except for the a_1 coefficient of the m_{sand}* pedotransfer function. However, even in this case, the impact of C_{hmin} on the a_1 coefficient is much lower than the confidence interval given by the bootstrapping, indicating that the relatively small number of soils we considered (as in other studies, e.g. Lu et al. (2007)) is a larger source of uncertainty.

Moreover, uncertainties in the f_{clay}, f_{silt}, f_{gravel}, or f_{SOM} fractions may be caused by (1) the natural heterogeneity of soil properties, (2) the living root biomass, (3) stones that may not be accounted for in the gravel fraction.

In particular, during the installation of the probes, it was observed that stones are present at some stations. Stones are not evenly distributed in the soil, and it is not possible to investigate whether the soil area where the temperature probes were inserted contains stones as it must be left undisturbed.

The grasslands considered in this study are not intensively managed. They consist of set-aside fields cut once or twice a year. Calvet et al. (1999) gave an estimate of 0.160 kg m^{-2} for the root dry matter content of such soils for a site in southwestern France, with most roots contained in the 0.25m top soil layer. This represents a gravimetric fraction of organic matter smaller than 0.0005 kg kg^{-1}, i.e. less than 4% of the lowest m_{SOM} values observed in this study (0.013 kg kg^{-1}) or less than 5% of f_{SOM} values. We checked that increasing f_{SOM} values by 5% has negligible impact on heat capacity and on the λ retrievals.

4.2. Can the new λ_{sat} model be applied to other soil types ?

The λ_{sat} values we obtained are consistent with values reported by other authors. In this study, λ_{sat} values ranging between 1.26 $Wm^{-1}K^{-1}$ and 2.80 $Wm^{-1}K^{-1}$ are found (Table 2). Tarnawski et al. (2011) gave λ_{sat} values ranging between 2.5 $Wm^{-1}K^{-1}$ and 3.5 $Wm^{-1}K^{-1}$ for standard sands. Lu et al. (2007) gave λ_{sat} values ranging between 1.33 $Wm^{-1}K^{-1}$ and 2.2 $Wm^{-1}K^{-1}$.

A key component of the λ_{sat} model is the pedotransfer function for quartz (Eq. (12)). The f_q pedotranfer functions we propose are based on available soil characteristics. The current global soil digital maps provide information about SOM, gravels and bulk density (Nachtergaele et al., 2012). Therefore, using Eq. (1) and Eqs. (6)-(12) at large scale is possible, and porosity can be derived from Eq. (1). On the other hand, the suggested f_q pedotranfer functions are obtained for temperate grassland soils containing a rather large amount of organic matter, and are valid for $m_{\mathrm{sand}}/m_{\mathrm{SOM}}$ ratio values lower than 40 (Table 2). These equations should be evaluated for other regions. In particular, hematite has to be considered together with quartz for tropical soils (Churchman and Lowe, 2012). Moreover, the pedotransfer function we get for θ_{sat} (Eq. (13)) and we use to conduct the sensitivity study of Sect. 3.3, is valid for the specific sites we considered. Eq. (13) cannot be used to predict porosity in other regions.

In order to assess the applicability of the pedotransfer function for quartz obtained in this study, we used the independent data from Lu et al. (2007) and Tarnawski et al. (2009), for ten Chinese soils (see Supplement 4 and Table S4.1). These soils consist of reassembled sieved soil samples and contain no gravel, while our data concern undisturbed soils. Moreover, most of these soils contain very little organic matter and the $m_{\mathrm{sand}}/m_{\mathrm{SOM}}$ ratio can be much larger that the $m_{\mathrm{sand}}/m_{\mathrm{SOM}}$ values measured at our grassland sites. For the 14 French soils used to determine pedotransfer functions for quartz, the $m_{\mathrm{sand}}/m_{\mathrm{SOM}}$ ratio ranges from 3.7 to 37.2 (Table 2). Only three soils of Lu et al. (2007) present such low values of $m_{\mathrm{sand}}/m_{\mathrm{SOM}}$. The other seven soils of Lu et al. (2007) present $m_{\mathrm{sand}}/m_{\mathrm{SOM}}$ values ranging from 48 to 1328 (see Table S4.1).

We used λ_{sat} experimental values derived from Table 3 in Tarnawski et al. (2009) to calculate Q and f_{q} for the ten Lu et al. (2007) soils. These data are presented in Supplement 4. Figure S4.1 shows the statistical relationship between these quantities and m_{sand}. Very good correlations of Q and f_{q} with m_{sand} are observed, with r^2 values of 0.72 and 0.83, respectively. This is consistent with our finding that f_{q} is systematically better correlated to soil characteristics than Q (Sect. 3.2). The pedotransfer functions derived from French soils tend to overestimate f_{q} for the Lu et al. (2007) soils, especially for the seven soils presenting $m_{\mathrm{sand}}/m_{\mathrm{SOM}}$ values larger than 40. Note that Lu et al. (2007) obtained a similar result for coarse-textured soils with their model, which assumed $Q = m_{sand}$. For the three other soils, presenting m_{sand}/m_{SOM} values smaller than 40, f_q MAE values are given in Table 4. The best MAE score (0.071 m^3m^{-3}) is obtained for the m_{sand}* predictor of f_q.

These results are illustrated by Fig. 9 for the m_{sand} predictor of f_q. Figure 9 also shows the f_q and λ_{sat} estimates obtained using specific coefficients in Eq. (12), based on the seven Lu et al. (2007) soils presenting m_{sand}/m_{SOM} values larger than 40. These coefficients are given together with the scores in Table 6. Table 6 also present these values for other predictors of f_q. It appears that m_{sand} gives the best scores. The contrasting coefficient values between Table 6 and Table 3 (Chinese and French soils, respectively) illustrate the variability of the coefficients of pedotransfer functions from one soil category to another, and the m_{sand}/m_{SOM} ratio seems to be a good indicator of the validity of a given pedotransfer function.

On the other hand, the m_{sand}/m_{SOM} ratio is not a good predictor of f_q for the Lu et al. (2007) soils presenting m_{sand}/m_{SOM} values larger than 40, and r^2 presents a small value of 0.40 (Table 6). This can be explained by the very large range of m_{sand}/m_{SOM} values for these soils (see Table S4.1). Using $ln(m_{sand}/m_{SOM})$ instead of m_{sand}/m_{SOM} is a way to obtain a predictor linearly correlated to f_q. This is shown by Fig. S4.2 for the ten Lu et al. (2007) soils: the correlation is increased to a large extent ($r^2 = 0.60$).

4.3. Can m_{sand}-based f_q pedotransfer functions be used across soil types ?

Given the results presented in Tables 3, 4, and 6, it can be concluded that m_{sand} is the best predictor of f_q across mineral soil types. The m_{sand}/m_{SOM} predictor is relevant for the mineral soils containing the largest amount of organic matter.

Although the m_{sand}/m_{SOM} predictor gives the best r^2 scores for the 14 grassland soils considered in this study, it seems more difficult to apply this predictor to other soils, as shown by the high MAE score (MAE = 0.135 m^3m^{-3}) for the corresponding Lu et al. (2007) soils in Table 4. Moreover, the scores are very sensitive to errors in the estimation of m_{SOM} as shown by Table 5. Although the m_{sand}* predictor gives slightly better scores than m_{sand} (Table 4), the a_1 coefficient in more sensitive to errors in C_{hmin} (Table 3), and the bootstrapping reveals large uncertainties in a_0 and a_1 values.

The results presented in this study suggest that the m_{sand}/m_{SOM} ratio can be used to differentiate temperate grassland soils containing a rather large amount of organic matter ($3.7 < m_{sand}/m_{SOM} < 40$) from soils containing less organic matter ($m_{sand}/m_{SOM} > 40$). The m_{sand} predictor can be used in both cases to estimate the volumetric fraction of quartz, with the following a_0 and a_1 coefficient values in Eq. (12): 0.15 and 0.572 for m_{sand}/m_{SOM} ranging between 3.7 and 40 (Table 3), and 0.04 and 0.386 for $m_{sand}/m_{SOM} > 40$ (Table 6), respectively.

4.4. Prospects for using soil temperature profiles

Using standard soil moisture and soil temperature observations is a way to investigate soil thermal properties over a large variety of soils, as the access to such data is facilitated by online databases (Dorigo et al., 2013).

A limitation of the data set we used, however, is that soil temperature observations (T_i) are recorded with a resolution of ΔT_i = 0.1 °C only (see Sect. 2.1). This low resolution affects the accuracy of the soil thermal diffusivity estimates. In order to limit the impact of this effect, a data filtering technique is used (see Supplement 5) and D_h is retrieved with a precision of 18 %.

It can be noticed that if T_i data were recorded with a resolution of 0.03 °C (which corresponds to the typical uncertainty of PT100 probes), D_h could be retrieved with a precision of about 5 % in the conditions of Eq. (S5.3). Therefore, one may recommend to revise the current practise of most observation networks consisting in recording soil temperature with a resolution of 0.1 °C only. More precision in the λ estimates would permit investigating other processes of heat transfer in the soil such as those related to water transport (Rutten, 2015).

5. Conclusions

An attempt was made to use routine soil temperature and soil moisture observations of a network of automatic weather stations to retrieve instantaneous values of the soil thermal conductivity at a depth of 0.10 m. The data from the SMOSMANIA network, in southern France, are used. First, the thermal diffusivity is derived from consecutive measurements of the soil temperature. The λ values are then derived from the thermal diffusivity retrievals and from the volumetric heat capacity calculated using measured soil properties. The relationship between the λ estimates and the measured soil moisture at a depth of 0.10 m permits the retrieval of λ_{sat} for 14 stations. The Lu et al. (2007) empirical λ model is then used to retrieve the quartz volumetric content by reverse modelling. A number of pedotransfer functions is proposed for volumetric fraction of quartz, for the considered region in France. For the grassland soils examined in this study, the ratio of sand to SOM fractions is the best predictor of f_q. A sensitivity study shows that omitting gravels and the SOM information has a major impact on λ_{sat}. Eventually, an error propagation analysis and a comparison with independent λ_{sat} data from Lu et al. (2007) show that the gravimetric fraction of sand within soil solids, including gravels and SOM, is a good predictor of the volumetric fraction of quartz when a larger variety of soil types is considered.

Acknowledgements

We thank Dr. Xinhua Xiao (NC State University Soil Physics, Raleigh, USA), Dr. Tusheng Ren (China Agricultural University, Beijing, China), and a third anonymous referee, for their review of the manuscript and for their fruitful comments. We thank Dr. Aaron Boone (CNRM, Toulouse, France) for his helpful comments. We thank our Meteo-France colleagues for their support in collecting and archiving the SMOSMANIA data: Catherine Bienaimé, Marc Bailleul, Laurent Brunier, Anna Chaumont, Jacques Couzinier, Mathieu Créau, Philippe Gillodes, Sandrine Girres, Michel Gouverneur, Maryvonne Kerdoncuff, Matthieu Lacan, Pierre Lantuejoul, Dominique Paulais, Fabienne Simon, Dominique Simonpietri, Marie-Hélène Théron, Marie Yardin.

References

Abu-Hamdeh, N. H., and Reeder, R. C.: Soil thermal conductivity: effects of density, moisture, salt concentration, and organic matter, Soil Sci. Soc. Am. J., 64, 1285–1290, 2000.

Albergel, C., Rüdiger, C., Pellarin, T., Calvet, J.-C., Fritz, N., Froissard, F., Suquia, D., Petitpa, A., Piguet, B., and Martin, E.: From near-surface to root-zone soil moisture using an exponential filter: an assessment of the method based on in-situ observations and model simulations, Hydrol. Earth Syst. Sci., 12, 1323–1337, 2008.

Albergel, C., Calvet, J.-C., de Rosnay, P., Balsamo, G., Wagner, W., Hasenauer, S., Naeimi, V., Martin, E., Bazile, E., Bouyssel, F., and Mahfouf, J.-F.: Cross-evaluation of modelled and remotely sensed surface soil moisture with in situ data in southwestern France, Hydrol. Earth Syst. Sci., 14, 2177–2191, doi:10.5194/hess-14-2177-2010, 2010.

Bristow, K. L., Kluitenberg, G. J., and Horton R.: Measurement of soil thermal properties with a dual-probe heat-pulse technique, Soil Sci. Soc. Am. J., 58, 1288–1294, doi:10.2136/sssaj1994.03615995005800050002x, 1994.

Bristow, K. L.: Measurement of thermal properties and water content of unsaturated sandy soil using dual-probe heat-pulse probes, Agr. Forest Meteorol., 89, 75-84, 1998.

Calvet, J.-C., Bessemoulin, P., Noilhan, J., Berne, C., Braud, I., Courault, D., Fritz, N., Gonzalez-Sosa, E., Goutorbe, J.-P., Haverkamp, R., Jaubert, G., Kergoat, L., Lachaud, G., Laurent, J.-P., Mordelet, P., Olioso, A., Péris, P., Roujean, J.-L., Thony, J.-L., Tosca, C., Vauclin, M., Vignes, D.: MUREX: a land-surface field experiment to study the annual cycle of the energy and water budgets, Ann. Geophys., 17, 838-854, 1999.

Calvet, J.-C., Fritz, N., Froissard, F., Suquia, D., Petitpa,A., and Piguet, B.: In situ soil moisture observations for the CAL/VAL of SMOS: the SMOSMANIA network, International

Geoscience and Remote Sensing Symposium, IGARSS, Barcelona, Spain, 23–28 July 2007, 1196–1199, doi:10.1109/IGARSS.2007.4423019, 2007.

Chen, Y. Y., Yang, K., Tang, W., Qin, J., and Zhao, L.: Parameterizing soil organic carbon's impacts on soil porosity and thermal parameters for Eastern Tibet grasslands, Sci. China Earth Sci., 55 (6), 1001–1011, doi:10.1007/s11430-012-4433-0, 2012.

Churchman, G. J. and Lowe, D. J.: Alteration, formation, and occurrence of minerals in soils, in Huang, P. M., Li, C., Summer, M. E. (eds.), Handbook of soil sciences: properties and processes, Chapter 20, 40-42, isbn:978-1-4398-0306-6, CRC Press, Boca Raton (FL), 2012.

Côté, J. and Konrad, J.-M.: A generalized thermal conductivity model for soils and construction materials, Can. Geotech. J., 42, 443:458, doi:10.1139/T04-106, 2005.

Crank J., and Nicolson, P.: A practical method for numerical evaluation of solutions of partial differential equations of the heat-conduction type, Advances in Computational Mathematics, 6, 207-226, doi:10.1007/BF02127704, 1996.

Decharme, B., Brun, E., Boone, A., Delire, C., Le Moigne, P., and Morin, S.: Impacts of snow and organic soils parameterization on northern Eurasian soil temperature profiles simulated by the ISBA land surface model, The Cryosphere, 10, 853–877, doi:10.5194/tc-10-853-2016, 2016.

de Vries, D. A.: Thermal properties of soils, in W.R. Van Wijk (ed.), Physics of plant environment, pp. 210–235, North-Holland Publ. Co., Amsterdam, 1963.

Dong, Y., McCartney, J. S., and Lu, N.: Critical review of thermal conductivity models for unsaturated soils, Geotech. Geol. Eng., 33,2,207-221, doi:10.1007/s10706-015-9843-2, 2015.

Dorigo, W. A., Wagner, W., Hohensinn, R., Hahn, S., Paulik, C., Xaver, A., Gruber, A., Drusch, M, Mecklenburg, S., van Oevelen, P., Robock, A., and Jackson, T.: The International Soil Moisture Network: a data hosting facility for global in situ soil moisture measurements, Hydrol. Earth Syst. Sci., 15, 1675–1698, doi:10.5194/hess-15-1675-2011, 2011.

Draper, C., Mahfouf, J.-F., Calvet, J.-C., Martin, E., and Wagner, W.: Assimilation of ASCAT near-surface soil moisture into the SIM hydrological model over France, Hydrol. Earth Syst. Sci., 15, 3829–3841, doi:10.5194/hess-15-3829-2011, 2011.

Farouki, O. T.: Thermal properties of soils, Series on Rock and Soil Mechanics, 11, Trans. Tech. Pub., Rockport, MA, USA, 136 pp., 1986.

Johansen, O.: Thermal conductivity of soils. Ph.D. thesis, University of Trondheim, 236 pp., Available from Universitetsbiblioteket i Trondheim, Høgskoleringen 1, 7034 Trondheim, Norway, a translation is available at: http://www.dtic.mil/dtic/tr/fulltext/u2/a044002.pdf (last access January 2016), 1975.

Kersten, M. S.: Thermal properties of soils, University of Minnesota Engineering Experiment Station Bulletin, 28, 227 pp. [Available from University of Minnesota Agricultural Experiment Station, St. Paul, MN 55108], 1949.

Laanaia, N., Carrer, D., Calvet, J.-C., and Pagé, C.: How will climate change affect the vegetation cycle over France? A generic modeling approach, Climate Risk Management, 13, 31-42, doi:10.1016/j.crm.2016.06.001, 2016.

Lawrence, D. M., and Slater, A. G.: Incorporating organic soil into a global climate model, Clim. Dyn., 30, 145-160, doi:10.1007/s00382-007-0278-1, 2008.

Lu, S., Ren, T., Gong, Y., and Horton, R.: An improved model for predicting soil thermal conductivity from water content at room temperature, Soil Sci. Soc. Am. J., 71, 8-14, doi:10.2136/sssaj2006.0041, 2007.

Nachtergaele, F., van Velthuize, H., Verelst, L., Wiberg, D., Batjes, N., Dijkshoorn, K., van Engelen, V., Fischer, G., Jones, A., Montanarella, L., Petri, M., Prieler, S., Teixeira, E., and Shi, X.: Harmonized World Soil Database, Version 1.2, FAO/IIASA/ISRIC/ISS-CAS/JRC, FAO, Rome, Italy and IIASA, Laxenburg, Austria, available at:

http://webarchive.iiasa.ac.at/Research/LUC/External-World-soil-database/HWSD_Documentation.pdf (last access January 2016), 2012.

Parlange, M. B., Cahill, A. T., Nielsen, D. R., Hopmans, J. W., and Wendroth, O.: Review of heat and water movement in field soils, Soil Till. Res., 47, 5-10, 1998.

Parrens, M., Zakharova, E., Lafont, S., Calvet, J.-C., Kerr, Y., Wagner, W., and Wigneron, J.-P.: Comparing soil moisture retrievals from SMOS and ASCAT over France, Hydrol. Earth Syst. Sci., 16, 423–440, doi:10.5194/hess-16-423-2012, 2012.

Peters-Lidard, C.D., Blackburn, E., Liang, X., and Wood, E.F.: The effect of soil thermal conductivity parameterization on surface energy fluxes and temperatures, J. Atmos. Sci., 55, 1209–1224, 1998.

Rutten, M. M.: Moisture in the topsoil: From large-scale observations to small-scale process understanding, PhD Thesis, Delft university of Technology, doi:10.4233/uuid:89e13a16-b456-4692-92f0-7a40ada82451, available at: http://repository.tudelft.nl/view/ir/uuid:89e13a16-b456-4692-92f0-7a40ada82451/ (last access: January 2016), 2015.

Schelde, K., Thomsen, A., Heidmann, T., Schjonning, P., and Jansson, P.-E.: Diurnal fluctuations of water and heat flows in a bare soil, Water Resour. Res., 34, 11, 2919-2929, 1998.

Schönenberger, J., Momose, T., Wagner, B., Leong, W. H., and Tarnawski, V. R.: Canadian field soils I. Mineral composition by XRD/XRF measurements, Int. J. Thermophys., 33, 342–362, doi:10.1007/s10765-011-1142-4, 2012.

Sourbeer, J. J., and Loheide II, S. P.: Obstacles to long-term soil moisture monitoring with heated distributed temperature sensing, Hydrol. Process., 30, 7, 1017-1035, 2015.

Subin, Z. M., Koven, C. D., Riley, W. J., Torn, M. S., Lawrence, D. M., and Swenson, S. C.: Effects of soil moisture on the responses of soil temperatures to climate change in cold regions, J. Clim., doi:10.1175/JCLI-D-12-00305.1, 26, 3139-3158, 2013.

Tarara, J.M., and J.M. Ham: Measuring soil water content in the laboratory and field with dual-probe heat-capacity sensors, Agron. J., 89, 535–542, 1997.

Tarnawski, V. R., McCombie, M. L., Leong, W. H., Wagner, B., Momose, T., and Schönenberger J.: Canadian field soils II. Modeling of quartz occurrence, Int. J. Thermophys., 33, 843–863, doi:10.1007/s10765-012-1184-2, 2012.

Tarnawski, V. R., Momose, T., and Leong, W. H.: Assessing the impact of quartz content on the prediction of soil thermal conductivity, Géotechnique, 59, 4, 331–338, doi: 10.1680/geot.2009.59.4.331, 2009.

Yang, K., Koike, T., Ye, B., and Bastidas, L.: Inverse analysis of the role of soil vertical heterogeneity in controlling surface soil state and energy partition, J. Geophys. Res., 110, D08101, 15 pp., doi:10.1029/2004JD005500, 2005.

Zakharova, E., Calvet, J.-C., Lafont, S., Albergel, C., Wigneron, J.-P., Pardé, M., Kerr, Y., Zribi, M. : Spatial and temporal variability of biophysical variables in southwestern France from airborne L-band radiometry, Hydrol. Earth Syst. Sci., 16, 1725-1743, doi:10.5194/hess-16-1725-2012, 2012.

Zhang, X., Heitman, J., Horton, R., and Ren, T.: Measuring near-surface soil thermal properties with the heat-pulse method: correction of ambient temperature and soil–air interface effects, Soil Sci. Soc. Am. J., 78, 1575–1583, doi:10.2136/sssaj2014.01.0014, 2014.

Table 1 – Soil characteristics at 10 cm for the 21 stations of the SMOSMANIA network. Porosity values are derived from Eq. (1). Solid fraction values higher than 0.3 are in bold. The stations are listed from West to East (from top to bottom). ρ_d, θ_{sat}, f, and m, stand for soil bulk density, porosity, volumetric fractions, and gravimetric fractions, respectively. Soil particle fractions larger than 0.3 are in bold. Station full names are given in Supplement 1 (Table S1.1).

Station	ρ_d (kg m^{-3})	θ_{sat} (m^{3}m^{-3})	f_{sand} (m^{3}m^{-3})	f_{clay} (m^{3}m^{-3})	f_{silt} (m^{3}m^{-3})	f_{gravel} (m^{3}m^{-3})	f_{SOM} (m^{3}m^{-3})	m_{sand} (kg kg^{-1})	m_{clay} (kg kg^{-1})	m_{silt} (kg kg^{-1})	m_{gravel} (kg kg^{-1})	m_{SOM} (kg kg^{-1})
SBR	1680	0.352	**0.576**	0.026	0.013	0.002	0.032	**0.911**	0.041	0.020	0.003	0.024
URG	1365	0.474	0.076	0.078	**0.341**	0.005	0.025	0.149	0.153	**0.665**	0.009	0.024
CRD	1435	0.438	**0.457**	0.027	0.033	0.000	0.045	**0.848**	0.051	0.060	0.000	0.041
PRG	1476	0.431	0.051	0.138	0.138	0.214	0.028	0.092	0.250	0.248	**0.385**	0.025
CDM	1522	0.413	0.073	0.241	0.231	0.012	0.030	0.128	**0.422**	**0.404**	0.020	0.026
LHS	1500	0.416	0.102	0.202	0.189	0.051	0.039	0.181	**0.359**	**0.335**	0.091	0.034
SVN	1453	0.445	0.127	0.073	0.176	0.162	0.017	0.233	0.133	**0.322**	0.296	0.015
MNT	1444	0.447	0.135	0.066	0.230	0.102	0.020	0.248	0.121	**0.424**	0.188	0.018
SFL	1533	0.413	0.127	0.071	0.118	0.250	0.021	0.221	0.123	0.205	**0.434**	0.018
MTM	1540	0.405	0.110	0.081	0.076	0.297	0.032	0.189	0.140	0.131	**0.512**	0.027
LZC	1498	0.429	0.129	0.066	0.068	0.292	0.015	0.229	0.117	0.121	**0.519**	0.013
NBN	1545	0.401	0.063	0.135	0.075	0.290	0.035	0.109	0.232	0.130	**0.499**	0.030
PZN	1311	0.495	0.222	0.074	0.131	0.054	0.023	**0.450**	0.151	0.266	0.111	0.023
PRD	1317	0.494	0.038	0.052	0.069	**0.326**	0.021	0.076	0.105	0.139	**0.659**	0.021
LGC	1496	0.428	0.253	0.044	0.042	0.214	0.019	**0.451**	0.078	0.074	**0.380**	0.017
MZN	1104	0.560	0.212	0.037	0.045	0.097	0.049	**0.510**	0.089	0.109	0.234	0.057
VLV	1274	0.506	0.294	0.054	0.086	0.031	0.029	**0.614**	0.112	0.179	0.064	0.030
BRN	1630	0.379	0.105	0.009	0.016	**0.474**	0.016	0.171	0.015	0.027	**0.774**	0.013
MJN	1276	0.506	0.064	0.029	0.056	**0.317**	0.028	0.133	0.060	0.118	**0.661**	0.029
BRZ	1280	0.508	0.097	0.074	0.109	0.190	0.020	0.202	0.154	0.228	**0.396**	0.021
CBR	1310	0.501	0.120	0.057	0.068	0.241	0.013	0.243	0.116	0.139	**0.489**	0.013

Table 2 – Thermal properties of 14 grassland soils in southern France: λ_{sat}, f_q and Q retrievals using the λ model (Eqs. (7)-(9) and Eq. (10), respectively) for degree of saturation values higher than 0.4, together with the minimized RMSD between the simulated and observed λ values, and the number of used λ observations (n). The soils are sorted from the largest to the smallest ratio of m_{sand} to m_{SOM}. Station full names are given in Supplement 1 (Table S1.1).

Station	λ_{sat} ($Wm^{-1}K^{-1}$)	RMSD ($Wm^{-1}K^{-1}$)	n	f_q (m^3m^{-3})	Q (kg kg^{-1})	$\frac{m_{sand}}{m_{SOM}}$
SBR	2.80	0.255	6	0.62	0.96	37.2
LGC	2.07	0.311	20	0.44	0.77	26.6
CBR	1.92	0.156	20	0.44	0.88	18.4
LZC	1.71	0.107	20	0.29	0.51	17.3
SVN	1.78	0.163	20	0.34	0.61	15.4
MNT	1.96	0.058	20	0.42	0.76	13.8
BRN	1.71	0.131	20	0.25	0.40	13.5
SFL	1.57	0.134	20	0.22	0.37	12.5
MTM	1.52	0.095	20	0.21	0.35	7.0
URG	1.37	0.066	20	0.05	0.10	6.2
LHS	1.57	0.136	20	0.26	0.45	5.3
CDM	1.82	0.086	20	0.26	0.44	5.0
PRG	1.65	0.086	20	0.18	0.32	3.7
PRD	1.26	0.176	20	0.14	0.28	3.7

Table 3 – Coefficients of four pedotransfer functions of f_q (Eq. 12) for 14 soils of this study (all with $m_{sand}/m_{SOM} < 40$), together with indicators of the coefficient uncertainty, derived by bootstrapping and by perturbing the volumetric heat capacity of soil minerals (C_{hmin}). The best predictor is in bold.

Predictor of f_q	Coefficients for 14 soils		Confidence interval from bootstrapping		Impact of a change of $\pm 0.08\times10^6$ J m^{-3} K^{-1} in C_{hmin}	
	a_0	a_1	a_0	a_1	a_0	a_1
$\boldsymbol{m_{sand} / m_{SOM}}$	0.12	0.0134	[0.10,0.14]	[0.012,0.014]	[0.11,0.13]	[0.013,0.013]
m_{sand}*	0.08	0.944	[0.00,0.11]	[0.85,1.40]	[0.07,0.09]	[0.919,0.966]
m_{sand}	0.15	0.572	[0.08,0.17]	[0.54,0.94]	[0.14,0.17]	[0.55,0.56]
$1- \theta_{sat} - f_{sand}$	0.73	–1.020	[0.71,0.89]	[–1.38, –0.99]	[0.70,0.73]	[–1.00, –0.99]

(*) only m_{sand} values smaller than 0.6 kg kg^{-1} are used in the regression

Table 4 – Scores of four pedotransfer functions of f_q for 14 soils of this study, together with the scores obtained by bootstrapping, without the sandy SBR soil. The MAE score of these pedotransfer functions for three Chinese soils of Lu et al. (2007) for which m_{sand}/m_{SOM} < 40 is given (within brackets). The best predictor and the best scores are in bold.

Predictor of f_q	Regression scores			Bootstrap scores			Scores without SBR (and MAE for 3 Lu soils)		
	r^2	RMSD (m^3m^{-3})	MAE (m^3m^{-3})	r^2	RMSD (m^3m^{-3})	MAE (m^3m^{-3})	r^2	RMSD (m^3m^{-3})	MAE (m^3m^{-3})
$\boldsymbol{m_{sand} / m_{SOM}}$	**0.77**	**0.067**	0.053	**0.72**	**0.074**	**0.059**	**0.62**	**0.070**	0.057 (*0.135*)
m_{sand}*	0.74	0.072	**0.052**	0.67	0.126	0.100	0.56	0.075	**0.056** (***0.071***)
m_{sand}	0.67	0.081	0.060	0.56	0.121	0.084	0.56	0.075	**0.056** (*0.086*)
$1- \theta_{sat} - f_{sand}$	0.65	0.084	0.064	0.56	0.102	0.079	0.45	0.084	0.061 (*0.158*)

(*) only m_{sand} values smaller than 0.6 kg kg^{-1} are used in the regression

Table 5 – Ability of the Eqs. (10)-(13) empirical model to estimate λ_{sat} values for 14 soils and impact of changes in gravel and SOM volumetric content: f_{gravel} = 0 m^{3}m^{-3} and f_{SOM} = 0.013 m^{3}m^{-3} (the smallest f_{SOM} value, observed for CBR). r^2 values smaller than 0.60, RMSD values higher than 0.20 Wm^{-1}K^{-1}, and mean bias values higher (smaller) than +0.10 (–0.10) are in bold.

Model configuration	Predictor of f_q	r^2	RMSD (Wm^{-1}K^{-1})	Mean bias (Wm^{-1}K^{-1})
Model using θ_{sat} observations	m_{sand} / m_{SOM}	0.86	0.14	+0.01
	m_{sand}*	0.83	0.15	–0.01
	m_{sand}	0.81	0.16	–0.03
	$1 - \theta_{sat} - f_{sand}$	0.82	0.16	–0.03
Full model using θ_{satMOD} (Eqs. (13))	m_{sand} / m_{SOM}	0.85	0.14	+0.03
	m_{sand}*	0.85	0.14	–0.03
	m_{sand}	0.84	0.15	–0.03
	$1 - \theta_{sat} - f_{sand}$	0.82	0.16	–0.02
same with: f_{SOM} = 0.013 m^{3}m^{-3}	m_{sand} / m_{SOM}	**0.57**	**0.35**	**+0.20**
	m_{sand}*	0.83	0.15	+0.00
	m_{sand}	0.81	0.16	–0.02
	$1 - \theta_{sat} - f_{sand}$	0.83	0.15	–0.02
same with: f_{gravel} = 0 m^{3}m^{-3}	m_{sand} / m_{SOM}	0.87	0.19	**–0.12**
	m_{sand}*	0.70	**0.23**	**+0.11**
	m_{sand}	0.79	0.17	+0.04
	$1 - \theta_{sat} - f_{sand}$	0.81	0.17	+0.05
same with: f_{SOM} = 0.013 m^{3}m^{-3} and f_{gravel} = 0 m^{3}m^{-3}	m_{sand} / m_{SOM}	0.63	**0.31**	**+0.16**
	m_{sand}*	**0.52**	**0.36**	**+0.24**
	m_{sand}	**0.59**	**0.29**	**+0.16**
	$1 - \theta_{sat} - f_{sand}$	0.70	**0.25**	**+0.16**

(*) only m_{sand} values smaller than 0.6 kg kg^{-1} are used in the regression

Table 6 – Pedotransfer functions of f_q (Eq. 12) for 7 soils of Lu et al. (2007) with m_{sand}/m_{SOM} > 40. The best predictor and the best scores are in bold. The regression p-values are within brackets.

Predictor of f_q	Regression scores for 7 Lu soils with $m_{sand}/m_{SOM} > 40$			Coefficients	
	r^2 (*p-value*)	RMSD (m^3m^{-3})	MAE (m^3m^{-3})	a_0	a_1
m_{sand} / m_{SOM}	0.40 (*0.13*)	0.089	0.075	0.20	0.000148
m_{sand}*	0.82 (*0.005*)	0.073	0.054	0.07	0.425
$\boldsymbol{m_{sand}}$	**0.82 (*0.005*)**	**0.048**	**0.042**	0.04	0.386
$1-\theta_{sat}-f_{sand}$	0.81 (*0.006*)	0.050	0.043	0.44	–0.814

(*) only m_{sand} values smaller than 0.6 kg kg^{-1} are used in the regression

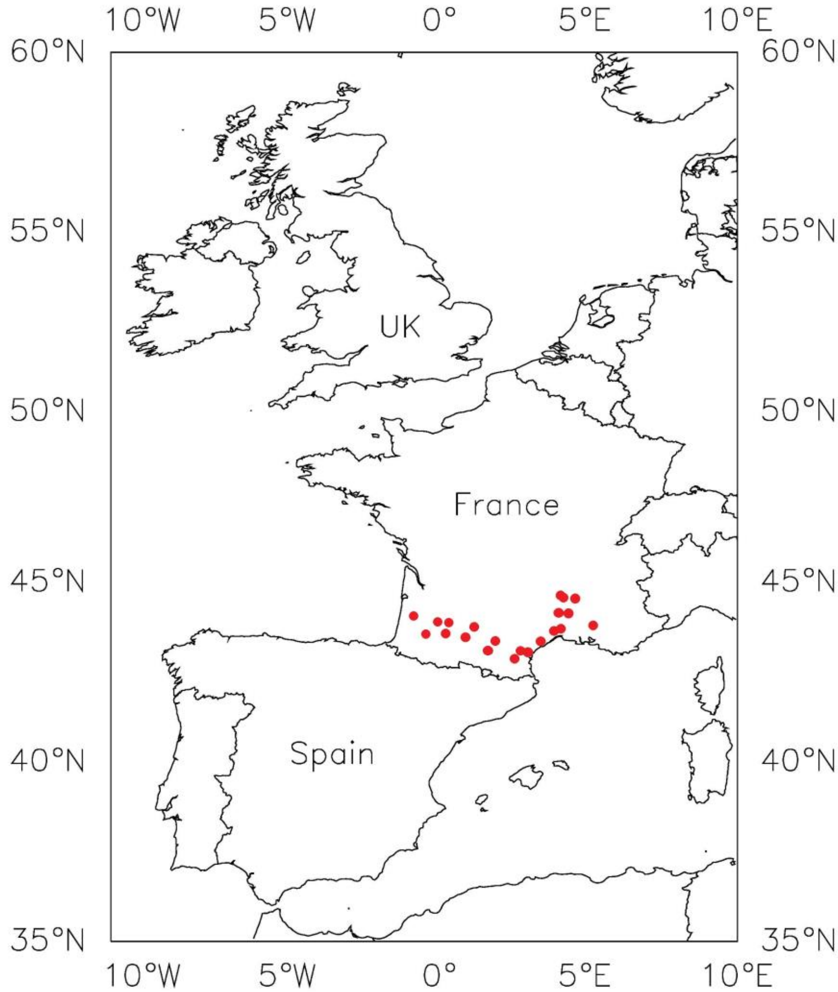

Fig. 1 – Location of the 21 SMOSMANIA stations in southern France (see station names in Supplement 1).

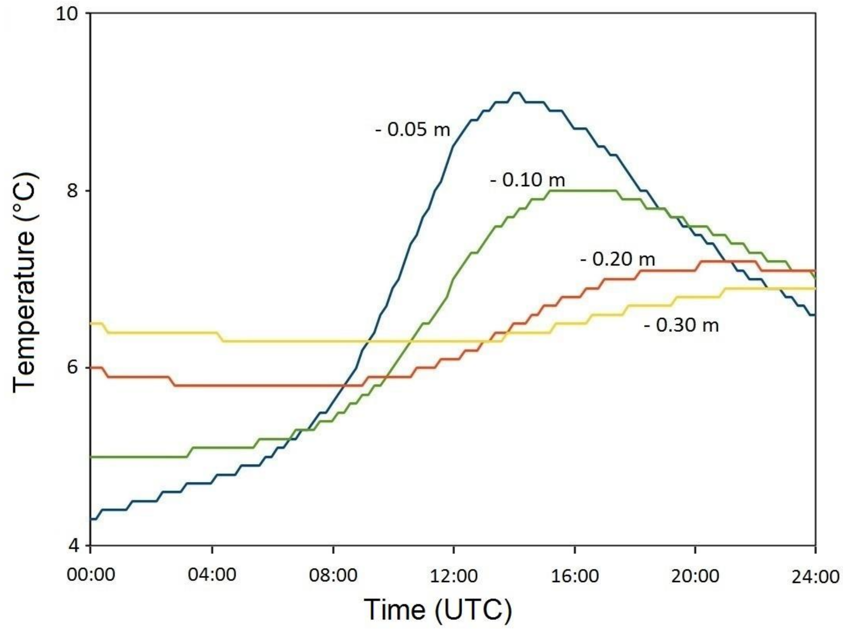

Fig. 2 – Soil temperature measured in wet conditions at the Saint-Félix-de-Lauragais (SFL) station on 23 February 2015, at depths of 0.05, 0.10, 0.20, and 0.30 m. Levelling is due to the low resolution of the temperature records (0.1°C).

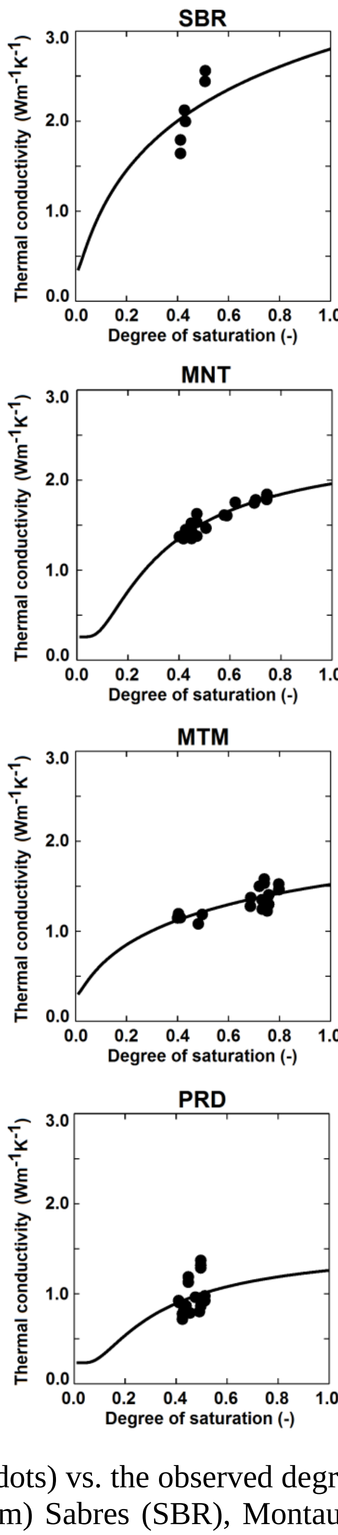

Fig. 3 – Retrieved λ values (dark dots) vs. the observed degree of saturation of the soil, at a depth of 0.10 m, for (from top to bottom) Sabres (SBR), Montaut (MNT), Mouthoumet (MTM), and Prades-le-Lez (PRD), together with simulated λ values from dry to wet conditions (dark lines).

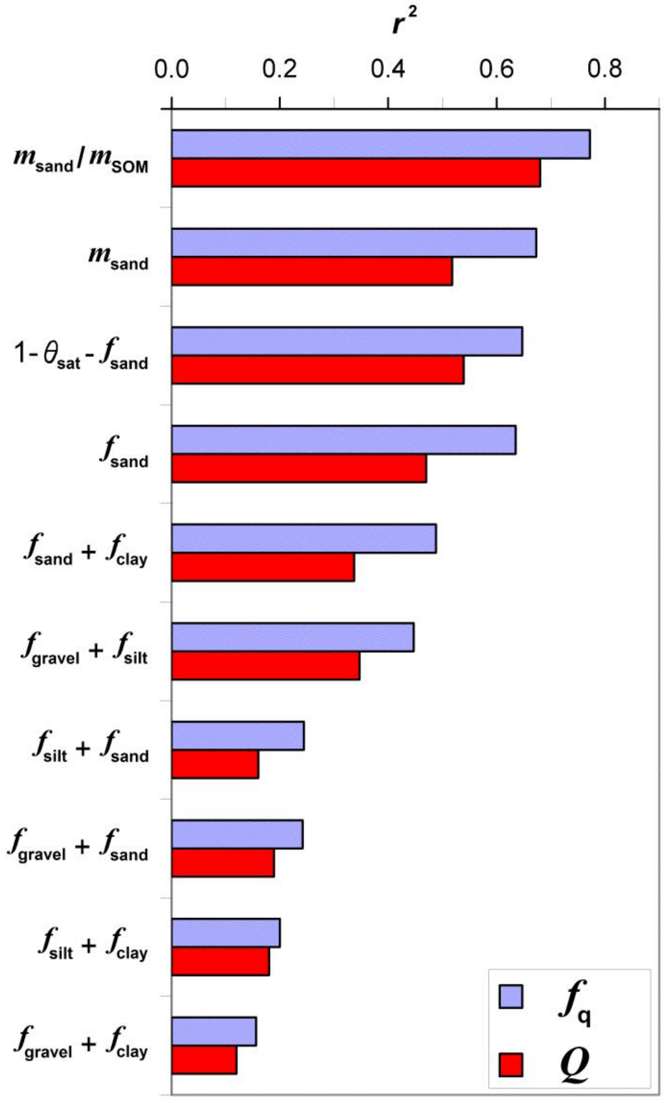

Fig. 4 – Fraction of variance (r^2) of gravimetric and volumetric fraction of quartz (Q and f_q, red and blue bars, respectively) explained by various predictors.

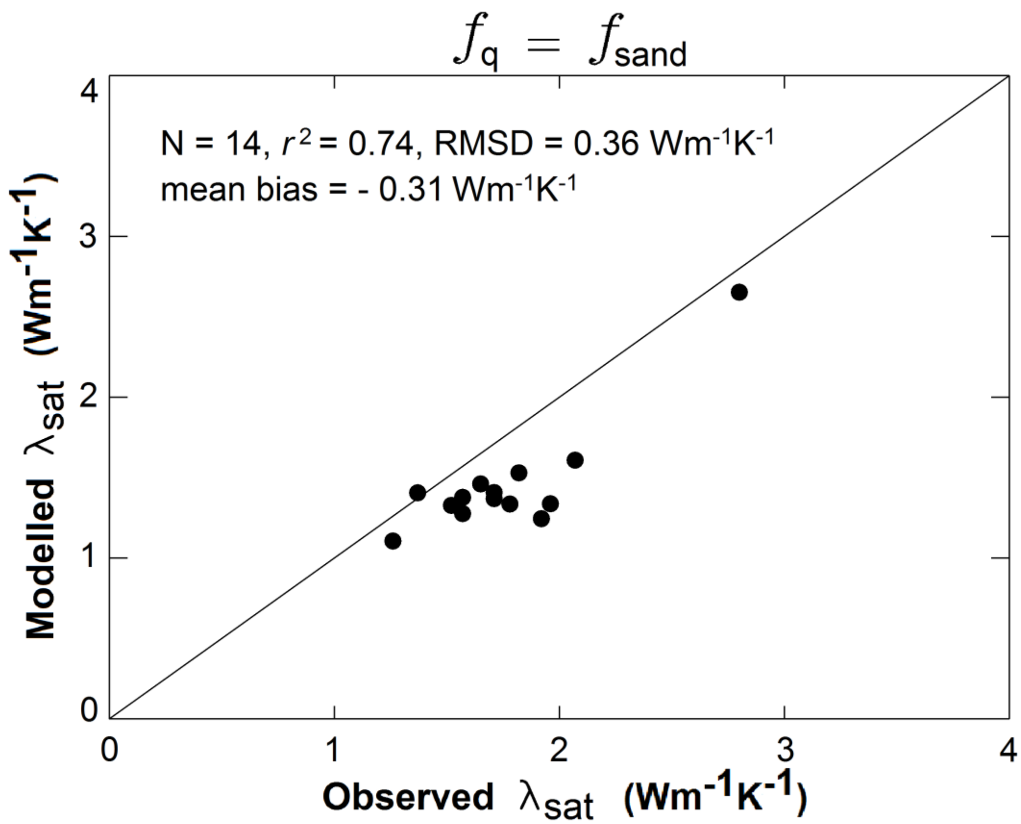

Fig. 5 – λ_{satMOD} values derived from volumetric quartz fractions f_q assumed equal to f_{sand}, using observed θ_{sat} values, vs. λ_{sat} retrievals.

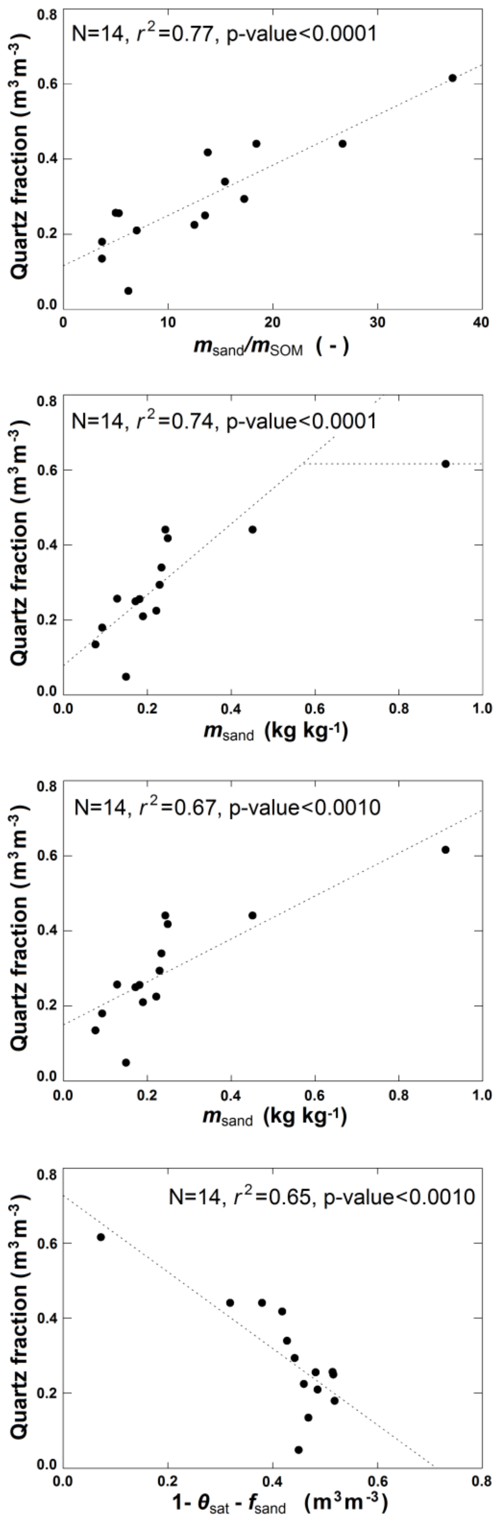

Fig. 6 – Pedotransfer functions for quartz: f_q retrievals (dark dots) vs. the four predictors of f_q given in Table 3. The modelled f_q values are represented by the dashed lines.

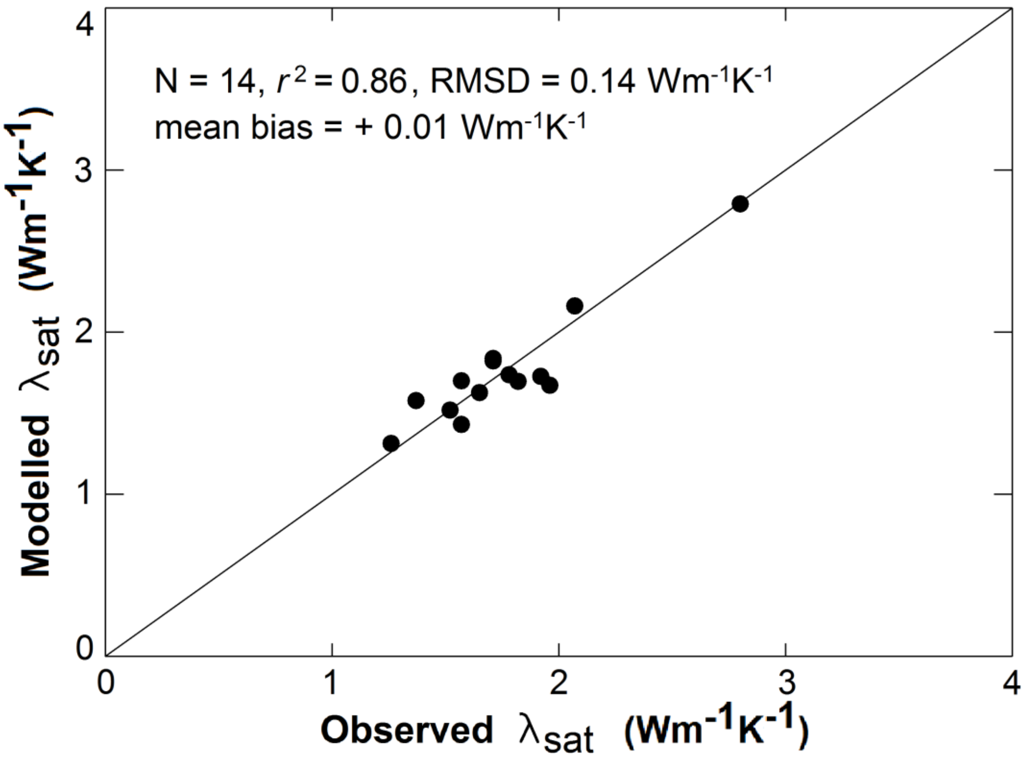

Fig. 7 – λ_{satMOD} values derived from the m_{sand} / m_{SOM} pedotransfer function for the volumetric quartz fractions, using observed θ_{sat} values, vs. λ_{sat} retrievals.

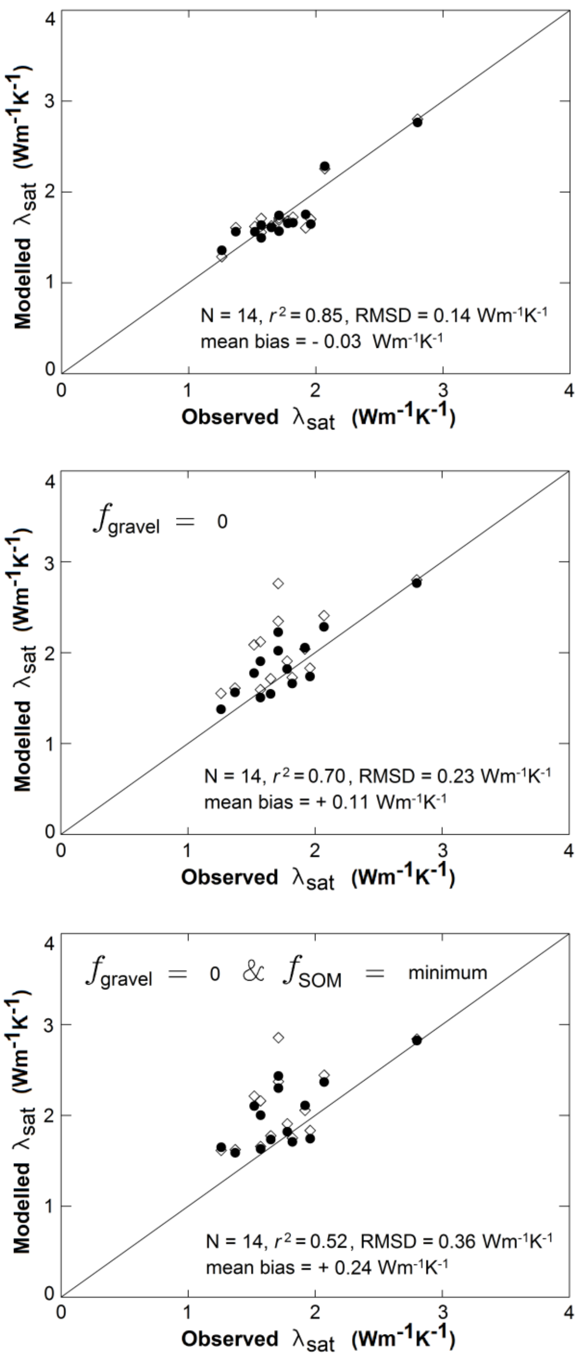

Fig. 8 – λ_{satMOD} values derived from the m_{sand}* pedotransfer function for the volumetric quartz fractions, using θ_{satMOD} (Eqs. (13)) or the observed θ_{sat} (dark dots and opened diamonds, respectively), vs. λ_{sat} retrievals: (top) full model, (middle) f_{SOM} = 0.013 m^{3}m^{-3}, (bottom) f_{SOM} = 0.013 m^{3}m^{-3} and f_{gravel} = 0 m^{3}m^{-3}. Scores are given for the θ_{satMOD} configuration.

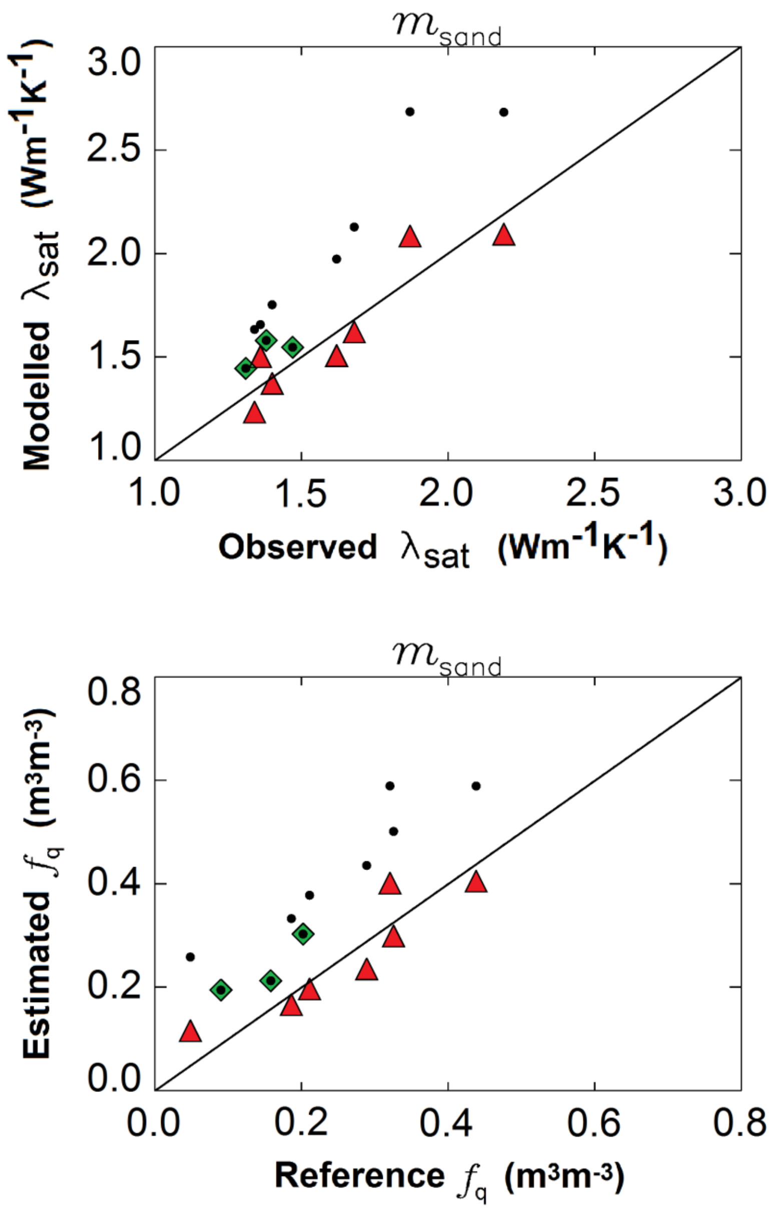

Fig. 9 – Estimated λ_{sat} and volumetric fraction of quartz f_{q} (top and bottom, respectively) vs. values derived from the λ_{sat} observations of Lu et al. (2007) given by Tarnawski et al. (2009) for 10 Chinese soils, using the gravimetric fraction of sand m_{sand} as a predictor of f_{q}. Dark dots correspond to the estimations obtained using the m_{sand} pedotransfer function for southern France and the three soils for which $m_{\text{sand}}/m_{\text{SOM}} < 40$ are indicated by green diamonds. Red triangles correspond to the estimations obtained using the m_{sand} pedotransfer function for the seven soils for which $m_{\text{sand}}/m_{\text{SOM}} > 40$ (see Table 6).